Article

Virtual Validation of In-Flight GNSS Signal Reception during Jamming for Aeronautics Applications

Veenu Tripathi [1,*] and Stefano Caizzone [1,2]

1 Institute of Communications and Navigation, German Aerospace Center (DLR), 82234 Wessling, Germany; stefano.caizzone@dlr.de
2 Information and Technology Department of Electrical Engineering, School of Computation, Technical University of Munich, 80333 Munich, Germany
* Correspondence: veenu.tripathi@dlr.de

Abstract: Accurate navigation is a crucial asset for safe aviation operation. The GNSS (Global Navigation Satellite System) is set to play an always more important role in aviation but needs to cope with the risk of interference, possibly causing signal disruption and loss of navigation capability. It is crucial, therefore, to evaluate the impact of interference events on the GNSS system on board an aircraft, in order to plan countermeasures. This is currently obtained through expensive and time-consuming flight measurement campaigns. This paper shows on the other hand, a method developed to create a virtual digital twin, capable of reconstructing the entire flight scenario (including flight dynamics, actual antenna, and impact of installation on aircraft) and predicting the signal and interference reception at airborne level, with clear benefits in terms of reproducibility and easiness. Through simulations that incorporate jamming scenarios or any other interference scenarios, the effectiveness of the aircraft's satellite navigation capability in the real environment can be evaluated, providing valuable insights for informed decision-making and system enhancement. By extension, the method shown can provide the ability to predict real-life outcomes even without the need for actual flight, enabling the analysis of different antenna-aircraft configurations in a specific interference scenario.

Keywords: antenna; GNSS; RF field measurement; jamming; digital twin; virtual flying; predictive analysis; interference analysis

1. Introduction

GNSS-based positioning is widely used in the modern era for safety-critical applications, especially in aeronautics. Quite little is known publicly about the RF environment characteristics that a GNSS system experiences while flying. One potential challenge in navigation systems is the possibility of a navigation receiver being jammed by a stronger electromagnetic signal [1–4]. It is a well-known and documented problem within the aviation community that GNSS receivers do not always function as desired. For aviation users, radio-frequency interference (RFI) created by jammers has long been touted as the main reason for the bad performance. The GNSS signals that reach the Earth's surface have extremely low power levels, ranging from −160 to −130 dBm, due to the distance of about 20,000 km between GNSS satellites and Earth's surface, increasing the susceptibility of GNSS signals to jamming risks [5,6]. A jammer has the ability to overpower the significantly weaker GNSS signals, resulting in the disruption of GNSS-based services within an area spanning several kilometers in radius. This interference can lead to a loss of the receiver's ability to process satellite signals, compromising the reliability and accuracy of the navigation system [7]. Also, limited knowledge of RF characteristics makes it more difficult to take proactive measures to mitigate the risk of interference and ensure the system's dependability [8].

Knowledge about the GNSS performance and reception characteristics during flight would be extremely valuable and would help in analyzing the response of GNSS systems

to eventual jamming events, even without flying, with clear benefits in terms of finance and effort. Multiantenna systems are known to be powerful countermeasures and have been vastly investigated in the latest years [9–13]. The authors have also proposed miniaturized antennas, capable of fitting into avionic footprints for single antenna elements, for optimal compliance with legacy systems [14,15]. In order to better study the flight behavior of these antennas, our institute in the German Aerospace Center (DLR) is performing a series of flight measurement campaigns at its Cochstedt site: the first one was performed in 2022, and then in 2023 and more shall follow in 2024. The results recorded with the single antennas of the DLR array (whose design was shown in [15]), will be used in this paper as a reference. Please note that the combined use of the antennas, such as to produce interference suppression, is not part of this work and will be the focus of a different paper. The focus of this paper on the other hand is to show the capability to predict the in-flight performance by a virtual validation tool.

In the literature, several authors have shown EM simulation tools for simulating the installed performance of the antenna on platforms/aircraft [16–18], but to our best knowledge, no work is publicly available showing the flying performance. In this article, we discuss the predictive tool that can well approximate beforehand the performance that will be obtained later on in-flight. Then we validate the simulation data with the data collected during flight trials that involve GNSS reception in the presence of jammer. This approach helps engineers predict the performance of antennas in challenging environments, enabling them to take proactive measures in advance without having to spend time and money on expensive flight tests.

This article consists of five sections. The introduction is provided in Section 1. Section 2 provides the details about DLR's measurement campaign whose data will be taken as a reference for the virtual validation. Installed performance analysis of the receiver antenna/jammer over aircraft/ground is explained in Section 3. Section 4 covers full-scenario simulation with two scenarios: (1) Jamming power level estimation, and (2) GNSS reception during jamming. Simulation and measurement results are discussed in Section 1. Finally, conclusions are given in Section 5.

2. DLR's Measurement Campaign

For the test scenario, flight data from the measurement campaign in Cochstedt, Germany, were taken as a reference. The flight route considered for the analysis is depicted in Figure 1. The measurements took place on 7 October 2022, between 12:26:26 and 12:29:48 UTC. The measurement campaign comprised the antenna described in [15] and is shown in Figure 2, which was installed on the DLR aircraft Do 228-101 D-CODE for flight tests.
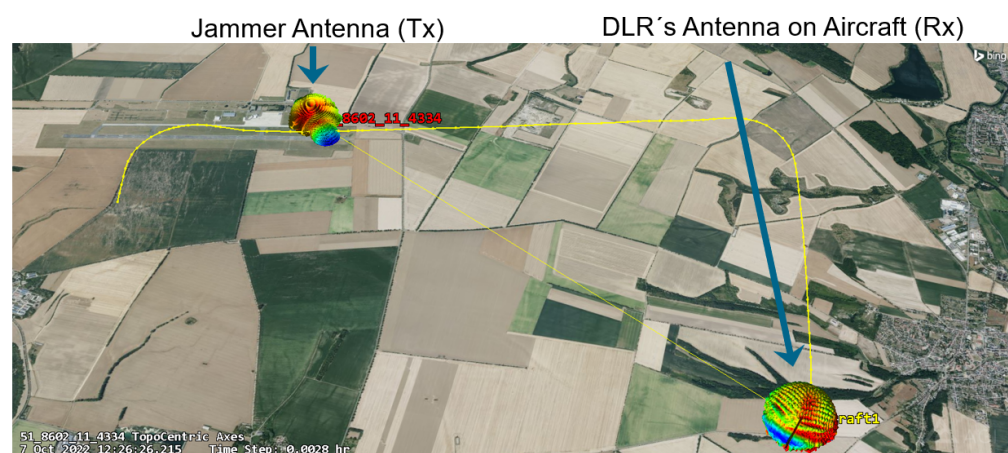
Figure 1. Flight route with jammer as transmitter and DLR's antenna as receiver.
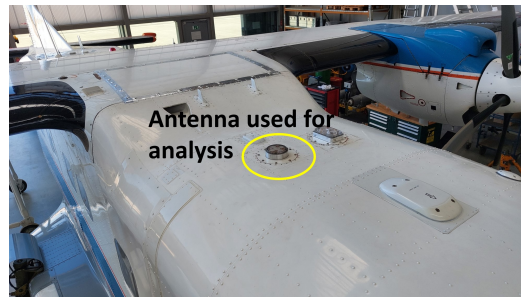
Figure 2. Antenna installed on the aircraft.

For this particular setup, the airborne antenna configuration consists of a compact array comprising four L1/E1 elements and one L5/E5a element. This compact array, with a 3.5-inch footprint, is well-suited for safety-of-life airborne applications due to its small size and the dual frequency capability it offers. For the current work, only signals from the four L1 elements are used (as single antennas, i.e., without any array processing).

A high gain GNSS helix antenna (MAT-18X8.5H1.1-1.6R-P-XN1), covering the full GNSS band from 1.1 to 1.66 GHz, from Matterwaves, Torrance, CA, USA, was used to radiate jamming signals. The antenna was placed at 51.86020550°, 11.43341470°, 225.27 m (or 51°51′36.7″ N 11°26′00.3″ E 180.490 MSL) and was transmitting with a power of 10.5 dBm. It was installed on the ground using tripod as shown in Figure 3.

Figure 3. Jammer antenna installed on the ground.

3. Installed Performance Analysis

The approach for assessing the installed performance involved a hybrid method. This hybrid approach, as depicted in Figure 4, utilizes both simulation results and measured data to accurately assess the antenna's performance when installed on the aircraft. First, the antenna design was carried out using commercial software Ansys HFSS (3D High Frequency Simulation Software) 2022 R2. Subsequently, the antenna was manufactured and measured in a semi-anechoic near-field chamber (MVG's Starlab) at the DLR facility. The measured electromagnetic fields in the anechoic chamber were then converted to equivalent currents on an enclosing box. These equivalent currents were used as the antenna source in electromagnetic simulations performed on a digital twin of the D-CODE airplane. A more detailed explanation of the approach is presented in [19].
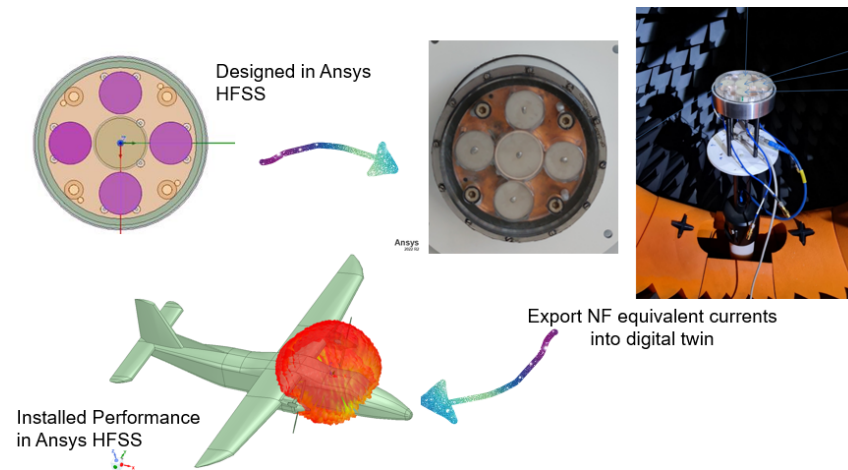
Figure 4. Hybrid installed performance scheme.

A simplified CAD (Computer Aided Design) model of the mentioned aircraft is available at the DLR facility; it was, therefore, used to simulate the installed performance of the antenna on the aircraft. Figure 5 illustrates both the original D-CODE aircraft and a simulated view of the antenna mounted on the aircraft using the Ansys HFSS. This allows for a visual comparison between the actual aircraft and the simulated antenna installation. Figure 6 shows the radiation pattern of one of the antenna elements of the selected antenna array measured in our Starlab and the radiation pattern obtained after simulating the installed performance of the antenna on aircraft. The reflections emanating from the aircraft contribute to the antenna's installed radiation pattern, resulting in a modification of the overall pattern of the installed antenna.
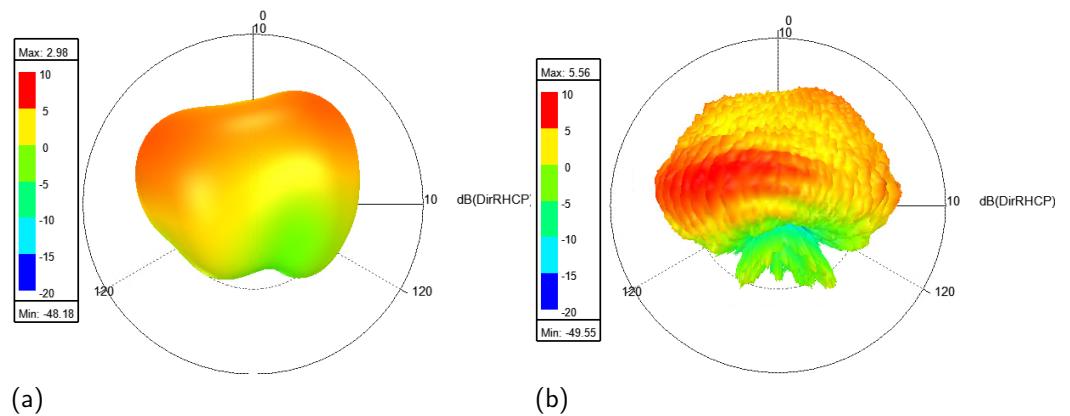

(a)
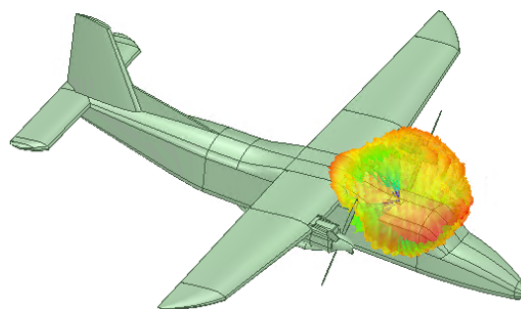
(b)

Figure 5. DLR's Dornier DO-228. (**a**) Original. (**b**) Simulated CAD model with installed antenna.

Figure 6. Radiation pattern of one antenna element. (**a**) Measured pattern in Starlab. (**b**) Installed performance on Aircraft.

A similar method has been applied to the jamming antenna, i.e., the GNSS helix antenna from Matterwaves. It was first measured in DLR's Starlab facility as shown in Figure 7. The pattern is then imported into HFSS to obtain the installed pattern of the antenna on the ground (see Figure 8). By considering the ground as a perfect electric conductor (PEC), we obtain insights into the maximum ground reflections, providing us with valuable information about multipath generation from the ground. A square on the ground measuring 100 m in length and breadth is selected with a jammer positioned at its center at a height of 1.6 m.

In addition to calculating the antenna's installed performance, we also integrate it into the system simulator from Ansys, i.e., STK (Systems Tool Kit) 12, to ensure optimal adherence and comparability to the data obtained from the measurement campaign. Ansys STK is software for digital mission engineering and systems analysis. It provides a physics-based modeling environment for analyzing platforms and payloads in a realistic mission context and provides canonical antenna patterns for the analysis. In our approach, however, the far fields of the simulated installed antenna performance, both for the receiver airborne antenna and jammer antenna, were imported into Ansys STK for a more realistic analysis of the full scenario. This technique provides a more accurate approximation of the actual power levels compared to simpler approaches such as using isotropic elements or built-in antennas in STK, which rely on simplified antenna pattern characteristics, and therefore, do not consider the pattern deformations due to installation in the scenario.
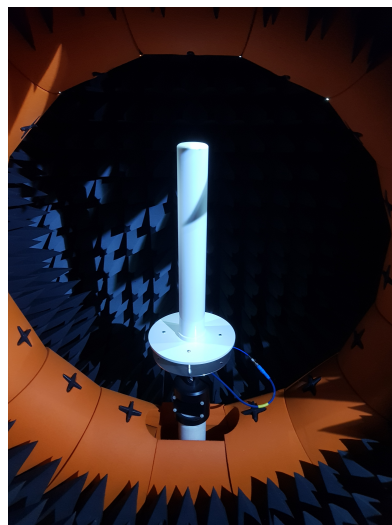
Figure 7. Jammer antenna in Starlab.

(a)

(b)
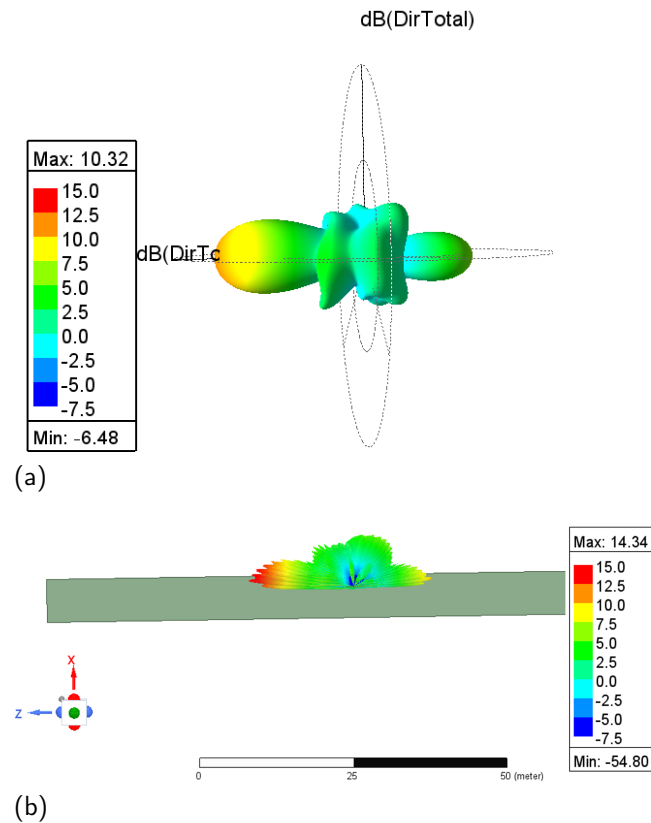
Figure 8. Radiation pattern of jammer antenna. (**a**) Measured pattern in Starlab. (**b**) Installed performance on PEC ground.

4. Full-Scenario Simulation

4.1. Scenario 1: Jamming Power Level Estimation

In the first scenario, we will analyze the amount of jamming power received at the airborne antenna during flight, as illustrated in Figure 1. In this case, the airborne antenna will receive jamming signals from the lower hemisphere, and hence, the installed performance (considering the shielding from the fuselage as well as the pattern distortions due to the installation) will be essential to obtain accurate information.

By analyzing the signals received from the jammer acting as the transmitter, it becomes possible to identify specific time intervals during which the jamming effect significantly impacts the reception of signals. These time intervals represent periods when the interference from the jammer has a notable influence on signal quality.

DLR's in-house developed hardware receiver, i.e., GALANT receiver [20,21], is used in the measurement campaign, whose simplified block diagram is shown in Figure 9. M (number of antenna elements) antennas are linked to M RF frontends, each housing an analog-to-digital converter (ADC), which feeds into the digital signal processing stage. For the sake of comparison between simulation and measurement, the measured power levels at the ADC input will be considered and compared with the jammer-to-noise (J/N) ratio (carrier-to-noise (C/N) ratio of the jammer) obtained from the simulation, as shown in Figure 10. Figure 11 shows the comparison between measured ADC power and simulated J/N in the specific time window where jammer power is highest at reception on the airborne side. As mentioned earlier, our signal reception setup utilizes four L1 elements, resulting in four antenna outputs that are available for comparison in the plots. A very good agreement between simulation and flight data can be observed. Having an estimate of the received interfering power anticipated in a flight scenario is highly beneficial in order to eventually plan countermeasures/adapt the interference suppression algorithms.
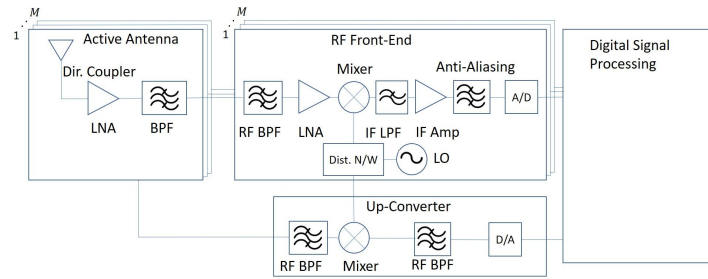
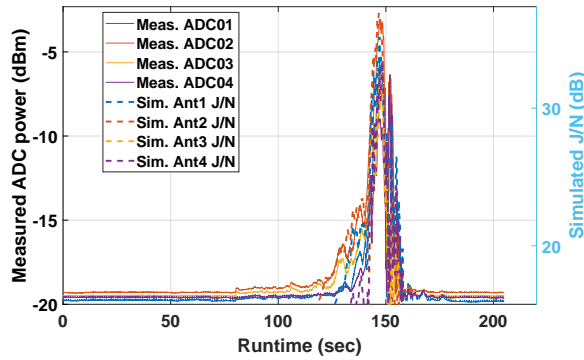**Figure 9.** Block diagram of the Galant array receiver.

Figure 10. Simulation and Measurement results for the flight route (full). (Solid lines–Measurement, Dashed lines–Simulation).
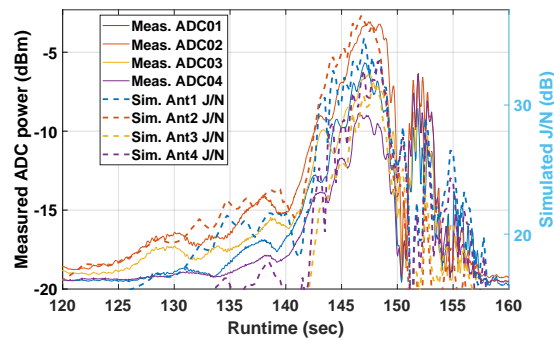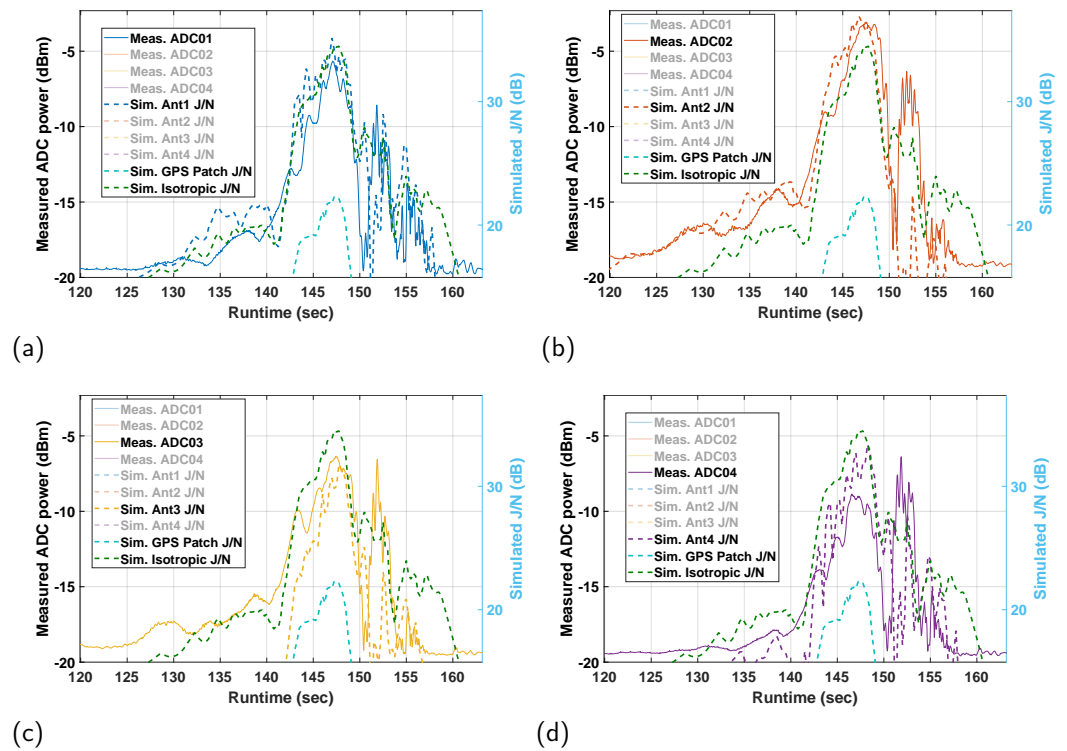

**Figure 11.** Simulation and Measurement results for the flight route (affected duration).

For a more detailed examination of the impact of jamming on individual antenna elements, Figure 12 provides a closer view of each antenna element. In order to obtain reference values, obtainable through easier system simulation, we have performed the same analysis employing not the sophisticated installed performance of the actual antenna, as shown in Figure 4, but a simplified antenna pattern, built-in in Ansys STK. In particular, we have analyzed the case of an isotropic antenna and a GPS "common patch" antenna. It is possible to notice in Figure 12 how the simplified simulations are incorrectly estimating the received power: in particular, the simplified patch antenna pattern (apparently a good candidate for the simulation) would totally underestimate the effect of the jammer, as it does not consider the backlobe effects. On the other hand, an isotropic pattern would better approximate the real behavior, but still (due to its strong simplification and the absence of any detailed information about the pattern deformation on the aircraft) provide less accurate results than the ones obtainable with the method we propose, properly considering the installed performance of the antenna.

Figure 12. Simulation and Measurement results for the flight route. (**a**) Ant.1. (**b**) Ant.2. (**c**) Ant.3. (**d**) Ant.4.

4.2. Scenario 2: GNSS Reception during Jamming

In the next scenario, we modeled the downlink portion of satellite transmission for GNSS transmitters as shown in Figure 13. GNSS transmitters are responsible for transmitting signals from GPS satellites to an aircraft receiver. This simulation allows us to study and analyze the behavior of the GNSS signal power level during jamming events. Both in the measurement campaign and in the virtual simulation, signals from 12 GPS satellites were received (see Figure 14).
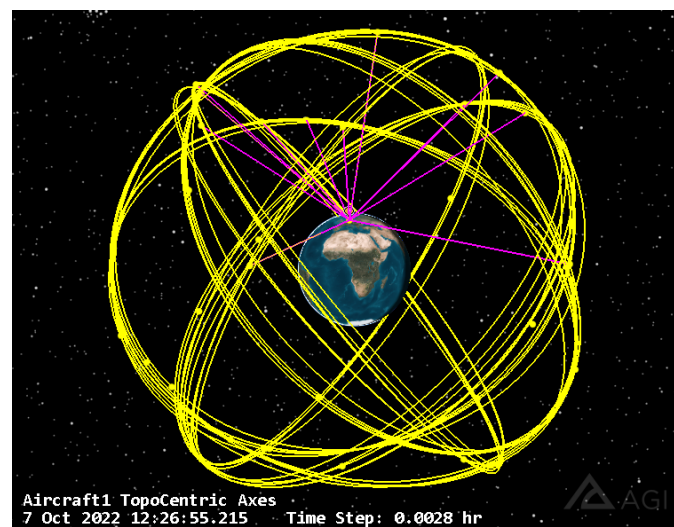
Figure 13. Simulated view of earth with GPS satellites (Yellow lines indicate the orbit of the satellites and pink lines indicate the connections between the GNSS satellites and the receiver).
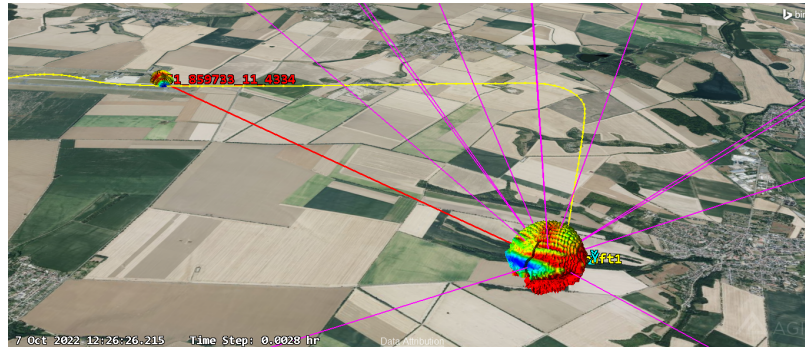
Figure 14. Connections made between GPS satellites and DLR's antenna (marked as pink lines).

To evaluate the quality of the GNSS signals, we used the metric called C/N_0, which stands for carrier-to-noise-density ratio. This metric is expressed in decibel-Hertz (dB-Hz) and represents the ratio of the carrier power (the power of the transmitted signal) to the noise power (unwanted signal components) per unit bandwidth. C/N_0 changes according to the mutual orientation of GPS satellites and receiving antenna. Moreover, in the case of jamming events, it will strongly decrease (as jamming effectively increases the not-wanted part of the signal). By measuring C/N_0, we can assess the signal strength and quality in the presence of interference.

The simulated and measured results, including the C/N_0 values at L1, are depicted in Figure 15. The figure depicts the congruent reception of signals from corresponding satellites during measurement and simulation. Figure 16 illustrates the specific time period when the jammer becomes effective. It is evident that during the time interval between 120 and 160 s, all (single) antennas experience a loss of signal tracking to the satellites. This loss of connection occurs because jamming is overpowering the signal.

The receiver employs a tracking threshold of 30 dB-Hz to monitor the satellites. When the signal strength drops beneath a predefined threshold, especially in the presence of jamming, the reception diminishes to zero, signifying a complete loss of signal. This decline is evident in the plots. Furthermore, the received carrier-to-noise ratio (C/N_0) values in the simulation setup also experience a significant decrease during the same time frame. This indicates that the simulation accurately reproduces the real-life scenario, as the observed loss of signal during the jamming period aligns with the simulation results.

The obtained results are shown in Figure 17 for some exemplary satellites and compared with the results of our method and with the measurement. To compare the different approaches quantitatively, we have calculated the approximate cumulative integral of the deviation of the simulation results of each approach from the measured data. The integral is defined as:

$$\int_a^b f(x)dx \approx \frac{b-a}{2N} \sum_{n=1}^{N} (f(x_n) + f(x_{n+1})), \tag{1}$$

where

$$f(x_n) = |(C/N_{0\text{Meas}} - C/N_{0\text{Sim}})|, \tag{2}$$

$a = x_1 < x_2 < ... < x_N < x_{N+1} = b$, and $(x_{n+1} - x_n)$ is the spacing between each consecutive pair of points. $C/N_{0\text{Meas}}$ denotes the measured C/N_0 values with Ant. 4 while $C/N_{0\text{Sim}}$ denotes the simulated values with Ant. 4 (as in our approach), GPS patch antenna or isotropic antenna. The integral results for the selected satellites with all intermediate values are shown in Figure 18. From Figure 17 it can be seen that in this case the isotropic antenna incorrectly predicts the signal drop before it actually occurs and Figure 18 confirms this as the integral value becomes very high (2.5–3 times) over the period analyzed as compared to our approach. On the other hand, the GPS common patch antenna pattern is more similar to our predictions and the measured data in this case (as expected, since the actual antennas have a pattern similar to the one of a patch), but underestimates signal (and jammer) reception at low elevations, as mentioned in the Scenario 1.

Most importantly, the reception obtained with both antennas, i.e., isotropic and GPS patch, remains consistently stable; the oscillations observed in the measurement, mostly due to reflections at aircraft or terrain level, are not modeled by the simplified patch/isotropic antenna simulations, while they can be better estimated by the validation tool proposed in the paper. The landscape upon which the jammer antenna is positioned and the aircraft on which the receiver antenna is mounted exert a significant influence on the ultimate radiation pattern achieved by the antennas.

The aspects outlined above clearly demonstrate the better way to predict the in-flight signal reception and show the advantage of our approach over conventional simulation using simplified antennas or without in-depth consideration of the installed performance.

Enhancing our comprehension of the scenario and conducting thorough analyses of antenna performance installed on platforms are integral in improving our ability to forecast GNSS reception. Furthermore, gaining deeper insights into the terrain characteristics of the scenario would yield additional advantages. Presently, our approach involves utilizing the PEC platform to optimize reflections for assessing antenna performance, both aerially and terrestrial. Employing appropriate platform materials could further augment our analytical capabilities in this regard.
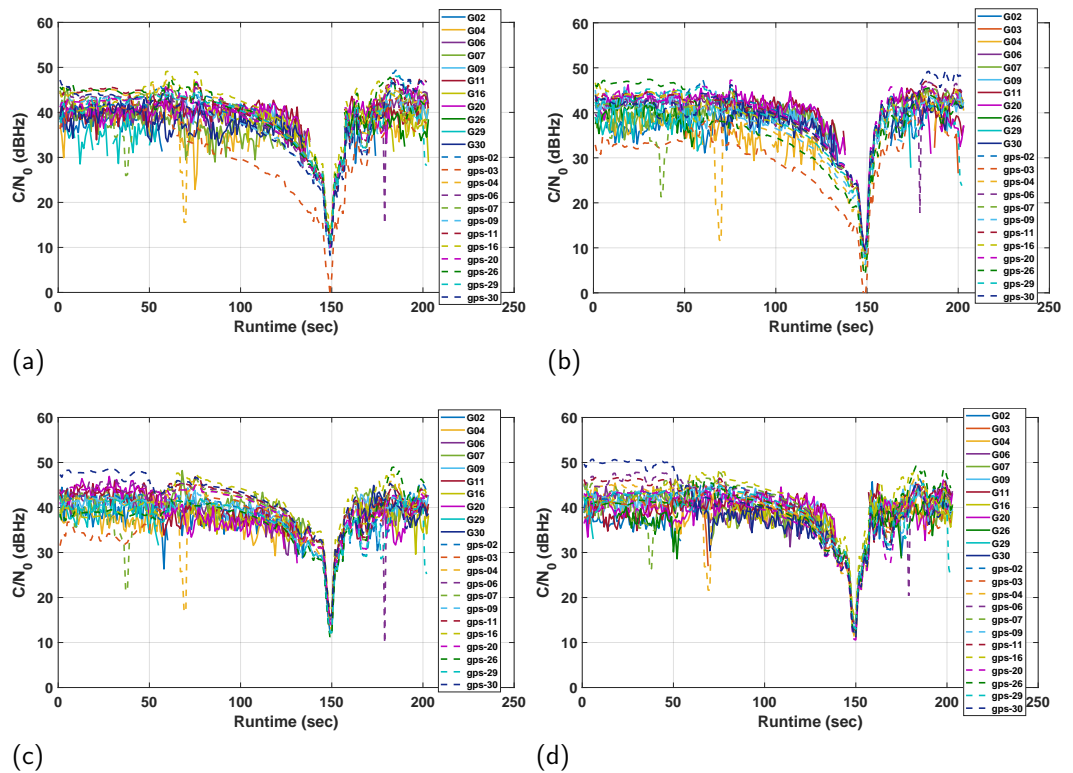
Figure 15. Simulation and Measurement results for the GNSS reception. (**a**) Ant.1. (**b**) Ant.2. (**c**) Ant.3. (**d**) Ant.4. (Solid lines–Measurement, Dashed lines–Simulation, GS and gps-S denotes measured and simulated GPS satellite number (S), respectively).
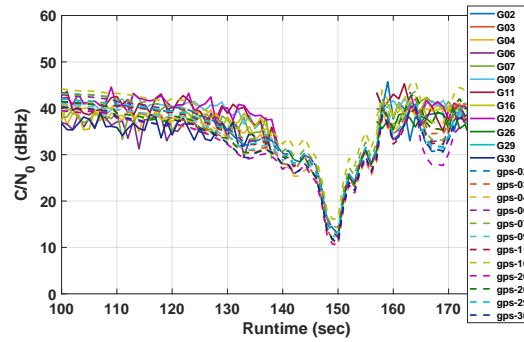
Figure 16. Simulation and Measurement results for the GNSS reception with Ant.4 (affected duration).
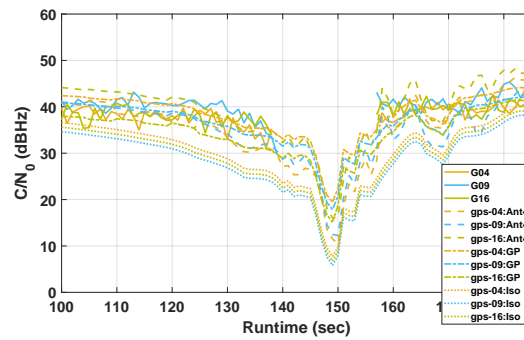

Figure 17. Simulation results for the GNSS reception with GPS patch antenna and Isotropic antenna (Solid lines–Measurement: Ant.4, Dashed lines–Simulation: Ant.4, DashDotDash lines–Simulation: GPS Patch, Dotted lines–Simulation: Isotropic).
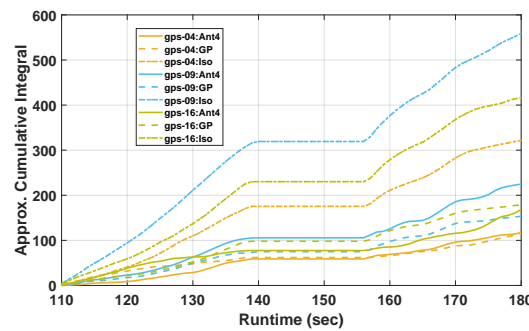

Figure 18. Approximate cumulative integral results for the deviation between the simulated GNSS reception and the measurements (Solid lines: Ant.4, Dashed lines: GPS Patch, DashDotDash: Isotropic).

5. Conclusions

This article has shown a virtual validation method able to predict the signal power received on the airborne side during flight. The method has been tested and validated with measurement data from a flight campaign, showing very good agreement between the simulated and measurement data, much better than the one obtainable when considering simplified antenna characteristics. By incorporating actual antenna measurement and installed performance analysis into the system flight scenarios, we can gain valuable insights into the performance to be expected in flight, even before flying. This approach allows for a more realistic representation of the conditions and parameters involved, enabling better insights and predictions for the test outcomes and saving a lot of time and money needed for multiple actual flight trials. This showcases the tool's significant capability as a predictive tool, enabling the planning of experiments or even virtually simulating various antenna+aircraft configurations while operating in specific interference scenarios to obtain results that closely approximate actual flight conditions.

References

1. Pokrajac, I.; Kozić, N.; Čančarević, A.; Brusin, R. Jamming of GNNS signals. *Sci. Tech. Rev.* **2018**, *68*, 18–24. [CrossRef]
2. Osechas, O.; Fohlmeister, F.; Dautermann, T.; Felux, M. Impact of GNSS-band radio interference on oper-ational avionics. *NAVIGATION J. Inst. Navig.* **2022**, *69*, navi.516.
3. Radio Frequency Interference to satellite navigation: An active threat for aviation? In *EUROCON-TROL Think Paper 9*; EURO-CONTROL: Brussels, Belgium, 2021.
4. Figuet, B.; Waltert, M.; Felux, M.; Olive, X. GNSS Jamming and Its Effect on Air Traffic in Eastern Europe. *Eng. Proc.* **2022**, *28*, 12.
5. Dinesh, S.; Faudzi, M.M.; Fitry, M.A.Z. Evaluation of the effect of radio frequency interference on Global Positioning System (GPS) accuracy via GPS simulation. *Def. Sci. J.* **2012**, *62*, 338–347.
6. Department of Army (DOA). Electronic Warfare in Operations. In *Army Field Manual 3–36*; Department of Army: Washington, DC, USA, 2009.
7. Borio, D.; Dovis, F.; Kuusniemi, H.; Presti, L.L. Impact and Detection of GNSS Jammers on Consumer Grade Satellite Navigation Receivers. *Proc. IEEE* **2016**, *104*, 1233–1245. [CrossRef]
8. Cuntz, M.; Konovaltsev, A.; Sgammini, M.; Hattich, C.; Kappen, G.; Meurer, M.; Hornbostel, A.; Dreher, A. Field test: Jamming the DLR adaptive antenna receiver. In Proceedings of the 24th International Technical Meeting of The Satellite Division of the Institute of Navigation (ION GNSS 2011), Portland, OR, USA, 19–23 September 2011; pp. 384–392.
9. Amin, M.G.; Sun, W. A novel interference suppression scheme for global navigation satellite systems using antenna array. *IEEE J. Sel. Areas Commun.* **2005**, *23*, 999–1012. [CrossRef]
10. Fernández-Prades, C.; Arribas, J.; Closas, P. Robust GNSS Receivers by Array Signal Processing: Theory and Implementation. *Proc. IEEE* **2016**, *104*, 1207–1220. [CrossRef]
11. Pérez-Marcos, E.; Caizzone, S.; Cuntz, M.; Konovaltsev, A.; Meurer, M. STAP Performance and Antenna Miniaturization in Multi-Antenna GNSS Receivers. In Proceedings of the 32nd International Technical Meeting of the Satellite Division of The Institute of Navigation (ION GNSS+ 2019), Miami, FL, USA, 16–20 September 2019; pp. 2575–2587.
12. Volakis, J.L.; O'Brien, A.J.; Chen, C.-C. Small and Adaptive Antennas and Arrays for GNSS Applications. *Proc. IEEE* **2016**, *104*, 1221–1232. [CrossRef]
13. Yinusa, K.A.; Marcos, E.P.; Caizzone, S. Robust Satellite Navigation by Means of a Spherical Cap Con-formal Antenna Array. In Proceedings of the 18th International Symposium on Antenna Technology and Applied Electromagnetics (ANTEM), Waterloo, ON, Canada, 19–22 August 2018; pp. 1–2.
14. Tripathi, V.; Elmarissi, W.; Caizzone, S. An ITAR-free Dual Frequency Antenna Array in the ARINC Footprint for Robust Aeronautical Navigation. In Proceedings of the 33rd International Technical Meeting of the Satellite Division of The Institute of Navigation (ION GNSS+ 2020), Denver, CO, USA, 21–25 September 2020.
15. Caizzone, S.; Buchner, G.; Circiu, M.-S.; Cuntz, M.; Elmarissi, W.; Pérez Marcos, E. A Miniaturized Multiband Antenna Array for Robust Navigation in Aerial Applications. *Sensors* **2019**, *19*, 2258. [CrossRef] [PubMed]
16. Yang, J.; Su, D.-L.; Zhao, X.-Y.; Guo, D.-D. Analysis of performance before and after GNSS antenna is installed on the airplane. In Proceedings of the 2008 8th International Symposium on Antennas, Propaga-tion and EM Theory, Kunming, China, 2–5 November 2008; pp. 352–355.
17. Jiménez, F.J.; Sendarrubias, M.A.; Moreno, J.A.R.; Gil, E.P. Modern electromagnetic simulation tools ap-plied to On-aircraft Antenna Integration. In Proceedings of the 2012 6th European Conference on Antennas and Propagation (EUCAP), Prague, Czech Republic, 26–30 March 2012; pp. 912–916.
18. Weinmann, F.; Knott, P.; Vaupel, T. EM simulation of installed antenna performance on land, aerial and maritime vehicles. In Proceedings of the IEEE Antennas and Propagation Society International Symposium (APSURSI), Orlando, FL, USA, 7–13 July 2013; pp. 2179–2180.
19. Caizzone, S.; Tripathi, V.; Hehenberger, S. Investigating GNSS Multipath in Aeronautic Applications Through Antenna Installed Performance. In Proceedings of the 2021 15th European Conference on Antennas and Propagation (EuCAP), Dusseldorf, Germany, 22–26 March 2021; pp. 1–5.

20. Heckler, M.V.T.; Cuntz, M.; Konovaltsev, A.; Greda, L.A.; Dreher, A.; Meurer, M. Development of Robust Safety-of-Life Navigation Receivers. *IEEE Trans. Microw. Theory Tech.* **2011**, *59*, 998–1005. [CrossRef]
21. Cuntz, M.; Konovaltsev, A.; Meurer, M. Concepts, Development and Validation of Multi-Antenna GNSS Receivers for Resilient Navigation. *Proc. IEEE* **2016**, *104*, 1288–1301. [CrossRef]